Supporting Information

# Nanowires Bending over Backward from Strain Partitioning in Asymmetric Core–Shell Heterostructures

*Ryan B. Lewis,* Pierre Corfdir,† Hanno Küpers, Timur Flissikowski, Oliver Brandt, and Lutz Geelhaar*

Paul-Drude-Institut für Festkörperelektronik, Hausvogteiplatz 5–7, 10117 Berlin, Germany

* Email: lewis@pdi-berlin.de

† Present address: ABB Corporate Research, 5405 Baden-Dättwil, Switzerland

This Supporting Information provides additional details on the partial thermal decomposition of GaAs nanowires, the Bi-induced formation of InAs three-dimensional (3D) islands on the {1$\bar{1}$0} sidewall facets of GaAs nanowires, analytical nanowire strain/bending calculations, and time-resolved photoluminescence (PL) measurements and the optical anisotropies of bent group-III-As-based core–multishell nanowires.

## Decomposition of GaAs nanowires

To increase the aspect ratio of the GaAs nanowire cores, the as-grown 75-nm-diameter nanowires were decomposed in the molecular beam epitaxy (MBE) chamber at 680 °C in the absence of any flux. Nanowire decomposition at these conditions has been previously reported.[1] Figure S1 shows scanning electron microscopy (SEM) images of the as-grown GaAs nanowire cores, as well as nanowires which have been partially decomposed for 3 min. The diameter and length before decomposition is 75 nm and 3.9 μm, respectively. While the length of the decomposed nanowires is not significantly different, the diameter is reduced to about 45 nm. The decomposition therefore increases the nanowire aspect ratio, in this case from 50 to 80. Increasing the decomposition time to 4.5 min results in nanowires with a diameter of about 30 nm.

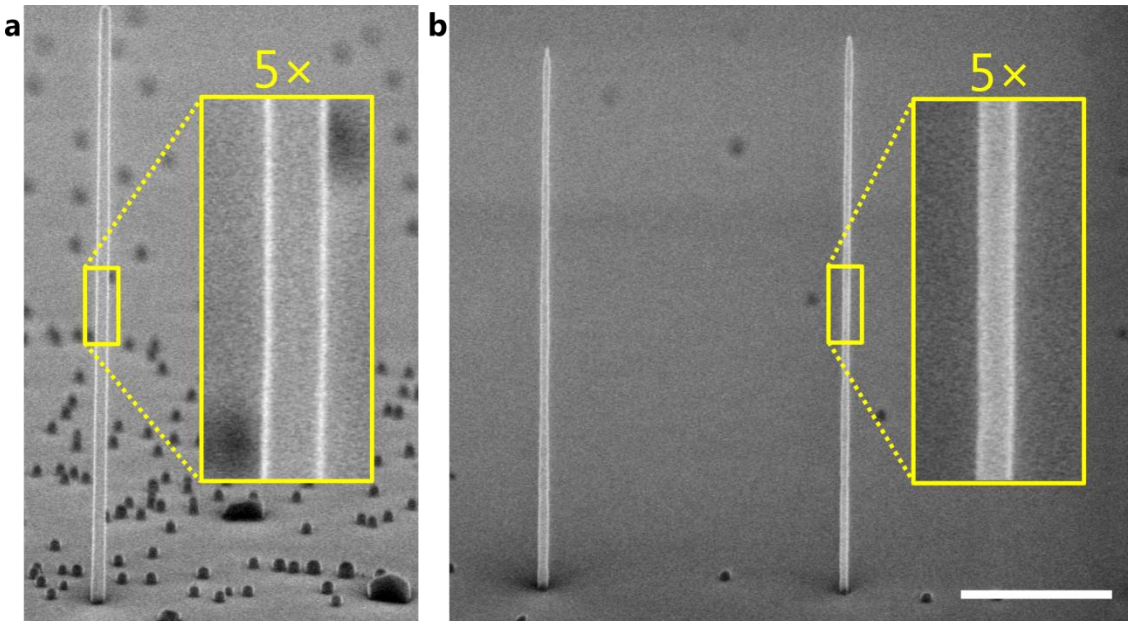


**Figure S1.** SEM images of selective area grown GaAs nanowire cores (a) before and (b) after decomposing for 3 min at 680 °C**.** (a) Before decomposition the nanowire diameter and length are about 75 nm and 3.9 μm, respectively. (b) After decomposition the nanowire diameter and length are about 45 nm and 3.7 μm, respectively. The viewing angle is 20° from the substrate plane. The scale bar corresponds to 1 μm and applies to both panels.

## Additional SEM images of bent nanowires

To further illustrate our ability to bend nanowires in predetermined directions, Figure S2 presents top-view SEM images of (a-b) the GaAs/$Al_{0.5}In_{0.5}As$ (45 nm/20 nm) nanowires from Figure 1, (c-d) the GaAs/$Al_{0.3}Ga_{0.7}As$/$Al_{0.5}In_{0.5}As$ nanowires from Figure 2 and (e-f) the quantum dot (QD) containing core–multishell nanowires from Figure 3 in the main text. In all panels, the nanowires are bent away from the direction from which the group III fluxes impinged during $Al_{0.5}In_{0.5}As$ deposition (indicated in the figure), corresponding to bending along the $[1\bar{1}0]$ direction in panels (a-b) and (e-f), and approximately along the $[2\bar{1}\ \bar{1}]$ direction in panels (c-d). In panel (a), the spacing of the GaAs/$Al_{0.5}In_{0.5}As$ nanowires is 5 μm and the wires are isolated, while in panel (b) the spacing is 1.5 μm and the wires are shown to overlap. In the insets of panels (d) and (e) the {110} nanowire facets are visible on the base of the nanowires. In panels

(c-f), suppression of the parasitic growth by the nanowire is visible on the substrate due to the shadowing of the group III fluxes by the nanowire.

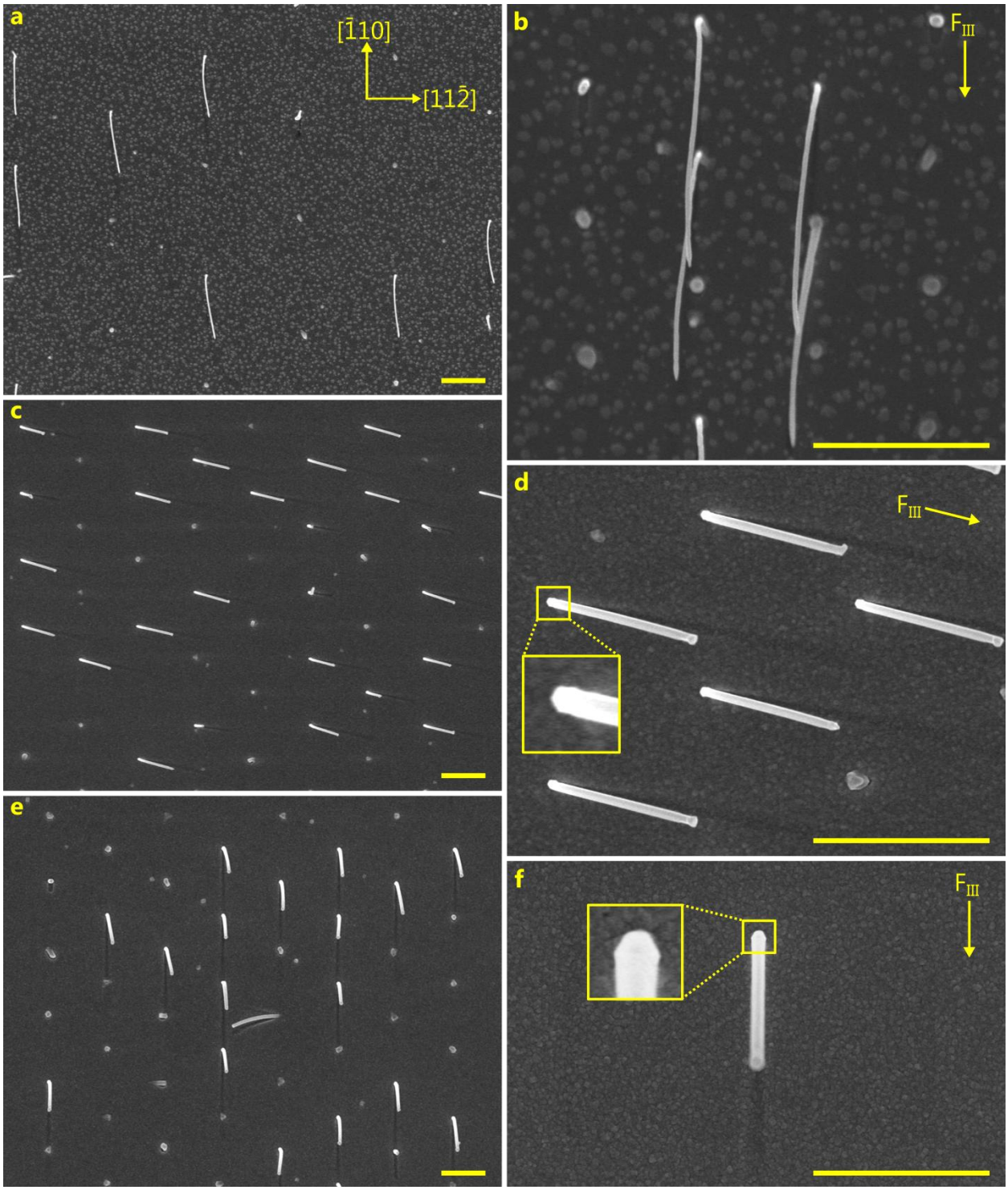

**Figure S2.** (a-b) Top-view SEM images of the bent nanowires from Figure 1 in the main text (45 nm core, 20 nm shell) illustrating both isolated and overlapping wires for nanowire spacings of (a) 5 μm and (b) 1.5 μm, respectively. (c-d) Top-view images of the bent $GaAs/Al_{0.3}Ga_{0.7}As/Al_{0.5}In_{0.5}As$ nanowires from Figure 2 in the main text. (e-f) Top-view images of the bent core–multishell nanowires from Figure 3 in the main text. The vertical nanowire yield in these fields varies from 33% to 43%. The nanowires are bent away from the direction from which the group III fluxes impinged during $Al_{0.5}In_{0.5}As$ deposition (indicated in panels (b), (d) and (e). The substrate crystallographic directions shown in (a) correspond to all panels. The scale bars correspond to 2 μm.

## Bi-induced formation of InAs 3D islands on GaAs nanowire sidewalls

We have previously reported that the presence of a Bi flux during InAs deposition on GaAs{110} planar surfaces and nanowire sidewalls provokes the formation of 3D islands, while deposition in the absence of Bi results in 2D growth.[2,3] As described in the methods section, for the deposition of InAs QDs on the nanowire sidewalls, In, Bi and $As_2$ were codeposited without substrate rotation. The source fluxes originate from different locations in the MBE chamber, and consequently the projection of each flux on the six $\{1\bar{1}0\}$ sidewall facets varies. It is therefore of interest to investigate how InAs deposition is distributed between the facets. The arrangement of the sources in our MBE system results in the In and $As_2$ fluxes being incident on opposite sidewall facets. Hence, a given nanowire sidewall is exposed to a direct flux from either In or $As_2$, but not both. The Bi cell is positioned next to the $As_2$ source (36° away, as illustrated in Figure S3b).

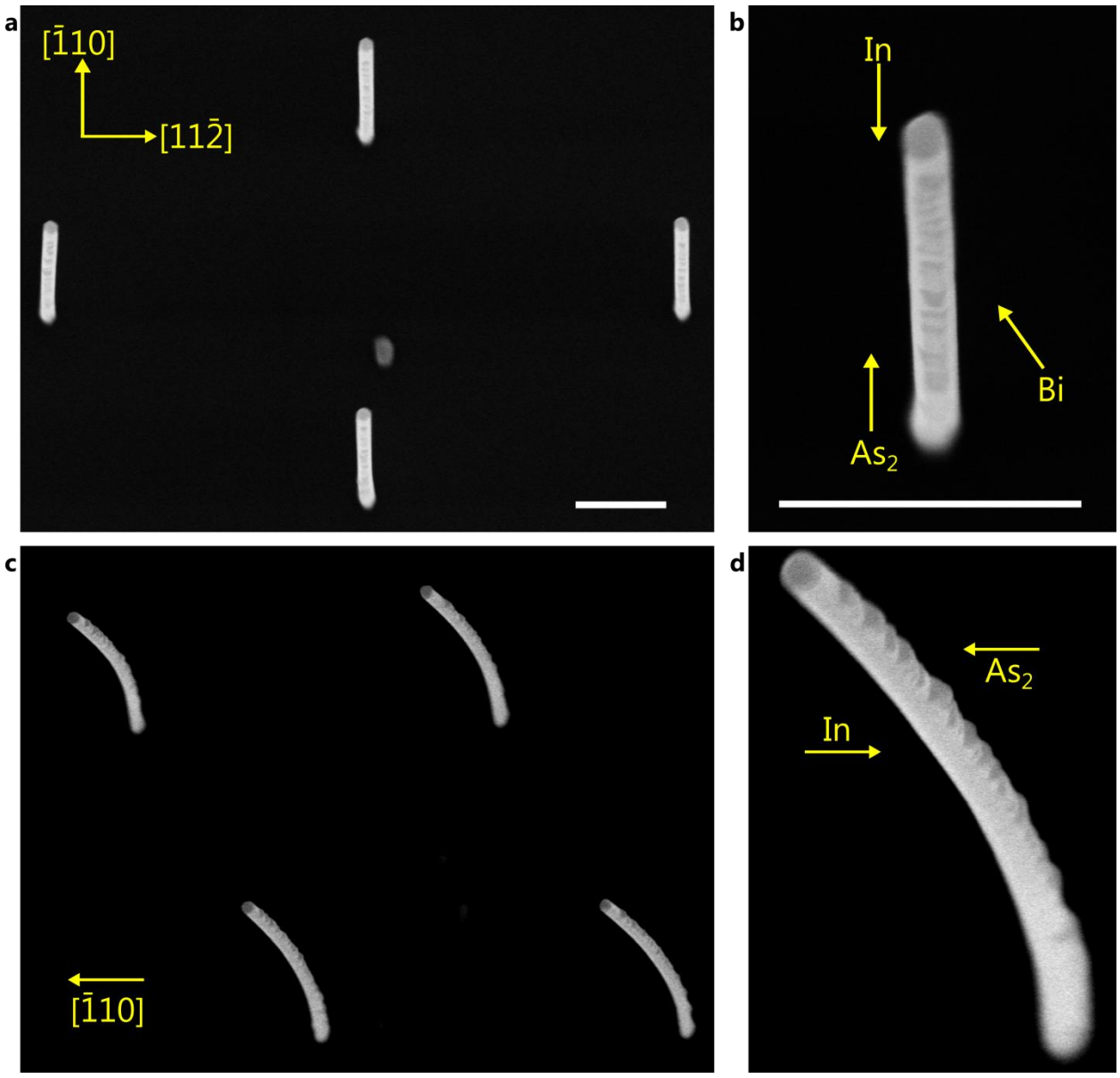


**Figure S3.** SEM images of GaAs nanowires after codepositing In, $As_2$ and Bi without substrate rotation. (a,b) Micrographs taken along the substrate normal, illustrating that the nanowires are bent in the [$\bar{1}$10] direction. (c,d) Micrographs taken at a viewing angle 20° away from the substrate normal in the [$\bar{1}\bar{1}$2] direction. The projections of the In, Bi and $As_2$ fluxes in the substrate plane are shown in (b) and (d). The scale bars in (a) and (c) apply also to (b) and (d), respectively, and correspond to 500 nm.

Figure S3 displays SEM images of 75-nm-diameter GaAs nanowires after deposition of InAs at the conditions described in the methods section (substrate temperature 420 °C, and In, Bi and $As_2$ fluxes corresponding to 0.1, 0.4 and 4 monolayers/s [ML/s] on planar GaAs(001),

respectively). In order to better visualize the resulting 3D islands, the InAs deposition time was increased from the 17 s used for samples in the main text to 60 s, corresponding to 1.2 nm of InAs deposition on the nanowire sidewalls. Micrographs taken at normal incidence to the substrate are shown in Figure S3a,b. The nanowires are tilted away from the normal in the $[\bar{1}10]$ direction, exposing the $(1\bar{1}0)$ sidewall on which 3D islands are visible (Figure S3b). We note that in Figure S3b, 3D formations are not observed on the left and right edges of the nanowires, and it appears that 3D growth was confined to the single $(1\bar{1}0)$ sidewall. Micrographs taken at a viewing angle of 20° away from the substrate normal in the $[\bar{1}\bar{1}2]$ direction are displayed in Figure S3c,d. These images clearly illustrate that 3D islands form on the $[1\bar{1}0]$-facing side of the nanowires. As shown in Figure S3b and S3d, this corresponds to the sidewall facet on which the $As_2$ flux was incident. No 3D growth is observed on the inner surfaces of the bent nanowires. Finally, the observed bending of the nanowires, a result of the strain induced in the GaAs core from the asymmetric InAs shell, is consistent with InAs deposition (2D and 3D) primarily occurring on the $[1\bar{1}0]$-facing side of the nanowires. These results indicate that In is sufficiently mobile to diffuse to the opposing side of the nanowires, where the $As_2$ flux is directly impinging and the chemical potential for In is the lowest. A similar effect has been observed for InAs growth on rippled surfaces, where surface gradients in the As-flux were found to drive selective area growth of QDs.[4] It is expected that As surface diffusion is negligible. These findings for InAs are in contrast to our asymmetric $Al_{0.5}In_{0.5}As$ shell deposition without Bi, where growth occurs on the side of the nanowire facing the group III sources. We note that previous reports of III-V MBE using Bi as a surfactant indicate that Bi increases adatom diffusion,[5] in contrast to the more common surfactants Te and Sb.[6,7]

## Analytical strain/bending calculations in asymmetric nanowire heterostructures

This section describes the analytical strain calculations discussed in the main text. For this discussion, we consider nanowires with the structures as shown schematically in Figure S4.

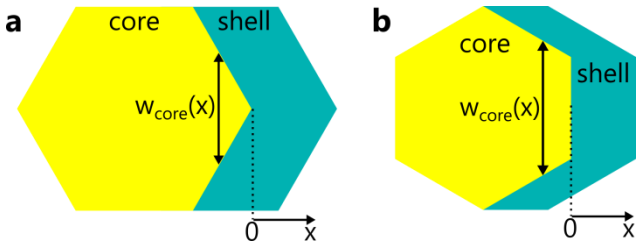


**Figure S4.** Schematic cross-sections of asymmetric core–shell nanowires for the two geometries considered in the main text.

The strain energy per unit length along the nanowire axis is given by

$$U = \frac{1}{2}\int E\varepsilon^2 dA \qquad \text{Eq. (1)},$$

where $E$ is Young's modulus, ε is the strain, and the integral is carried out over the cross sectional area of the nanowire with area element $dA$. Here, we consider only the axial component of strain $\varepsilon_{||}$. For the simple case of straight nanowires, the strain in the core $\varepsilon_{core}$ and in the shell $\varepsilon_{shell}$ are constant. As the core–shell interface is assumed to be coherent, the core and shell regions share the same lattice parameter along the nanowire axis, $a_{interface}$, and thus

$$\varepsilon_{core} = \frac{a_{interface} - a_{core}}{a_{core}} \qquad \text{Eq. (2)}$$

$$\varepsilon_{shell} = \frac{a_{interface} - a_{shell}}{a_{shell}} \qquad \text{Eq. (3)},$$

where $a_{core}$ and $a_{shell}$ are the unstrained axial lattice parameters of the core and shell materials, respectively. For straight nanowires, Eq. (1) yields

$$U = \frac{1}{2}[E_{core}\varepsilon_{core}^2 A_{core} + E_{shell}\varepsilon_{shell}^2 A_{shell}] \qquad \text{Eq. (4)},$$

where $A_{core}$ and $A_{shell}$ denote the cross sectional area of the core and shell, respectively. Minimizing $U$ with respect to $a_{interface}$, we obtain the following general expression for $a_{interface}$ for the case of straight nanowires

$$a_{interface,\ straight\ nanowires} = \frac{a_{core}a_{shell}(a_{core}A_{shell}E_{shell} + a_{shell}A_{core}E_{core})}{a_{core}^2 A_{shell}E_{shell} + a_{shell}^2 A_{core}E_{core}} \qquad \text{Eq. (5)}$$

For the case of bent nanowires, continuity of the axial lattice parameter at the core–shell interface is still required, however, now $\varepsilon_{||}$ varies linearly with distance $x$ across the interface. The resulting strains are given by

$$\varepsilon_{core} = \frac{a_{interface} - a_{core}}{a_{core}} + \frac{x}{r_o} \qquad \text{Eq. (6)}$$

$$\varepsilon_{shell} = \frac{a_{interface} - a_{shell}}{a_{shell}} + \frac{x}{r_o} \qquad \text{Eq. (7),}$$

where $x$ is the distance from the core–shell interface as illustrated in Figure S4 and $r_o$ is the bending radius of the nanowire at $x=0$. Assuming that the strain components only depend on $x$, the energy per unit length $U$ is given by Eq. (1) as

$$U = \frac{1}{2}\int \left( E_{core} w_{core}(x) \varepsilon_{core}^2(x) + E_{shell} w_{shell}(x) \varepsilon_{shell}^2(x) \right) dx \qquad \text{Eq. (8),}$$

where $w_{core}(x)$ and $w_{shell}(x)$ are the widths of the core and shell at position $x$, respectively (see Figure S4). Under the approximation that $E_{core}=E_{shell}$, we obtain $a_{interface}$ and $r_o$ by minimizing $U$ with respect to these parameters. The resulting nanowire curvature is shown as a function of shell thickness in Figure S5 for three core diameters, assuming a core–shell configuration as in Figure S4b (similar results are obtained for both geometries shown in Figure S4).

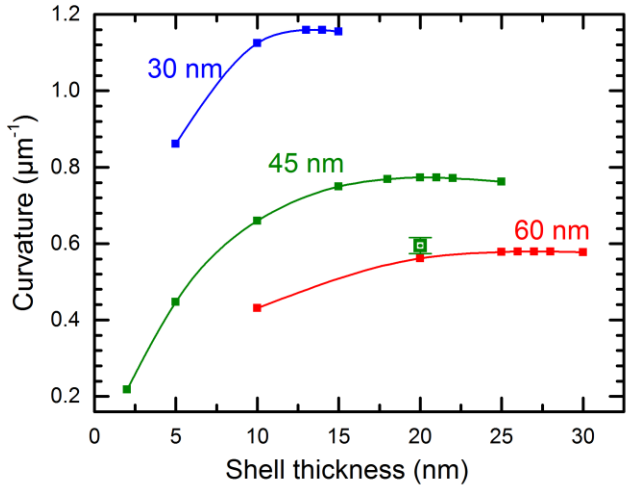


**Figure S5.** Calculated dependence of nanowire curvature on shell thickness for GaAs/$Al_{0.5}Ga_{0.5}As$ core–shell nanowires (configuration as in Figure S4b) with different core diameters. The core diameters $d_{core}$ are indicated for each data series in the figure. The minimum bending radius (maximum curvature) is achieved for a shell thickness of $0.45d_{core}$ and is equal to

about 29$d_{core}$. The hollow data point corresponds to the experimental curvature of the nanowires from Figure 1 in the main text (nominally 45 nm core).

## Time-resolved photoluminescence spectra

This section presents additional time-resolved PL experiments carried out on bent and straight GaAs/$Al_{0.3}Ga_{0.7}As$/$Al_{0.5}In_{0.5}As$ core–multishell nanowires at 10 K. Figure S6a displays time-resolved PL spectra extracted from the streak camera image shown in Figure 2e in the main text. Figure S6b displays the time evolution of the PL peak energy deduced from the Gaussian lineshape fits shown in Figure S6a. With increasing time delay, the drift of carriers toward the tensile-strained region of the GaAs core of bent nanowires results in a redshift and a narrowing of the PL signal.

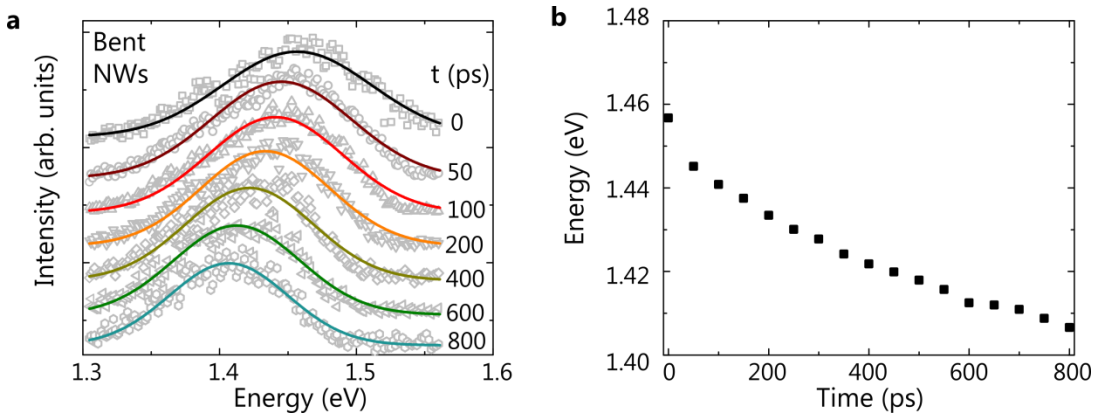


**Figure S6.** Time-resolved PL of bent GaAs/$Al_{0.3}Ga_{0.7}As$/$Al_{0.5}In_{0.5}As$ core–multishell nanowires. (a) Time-resolved PL spectra at 10 K extracted from the streak camera image shown in Figure 2e of the paper (symbols). The time delay after excitation is indicated for each spectrum in the figure. The spectra have been normalized and shifted vertically for clarity. The solid lines show the result of Gaussian lineshape fits. (b) Time evolution of the PL peak energy obtained from the lineshape fits.

For comparison with the bent nanowires, a streak camera image taken on straight GaAs/$Al_{0.3}Ga_{0.7}As$/$Al_{0.5}In_{0.5}As$ core–multishell nanowires is shown in Figure S7. The PL peak energy redshifts by only about 18 meV between 0 and 800 ps delay, which we attribute to carrier localization at stacking defects.

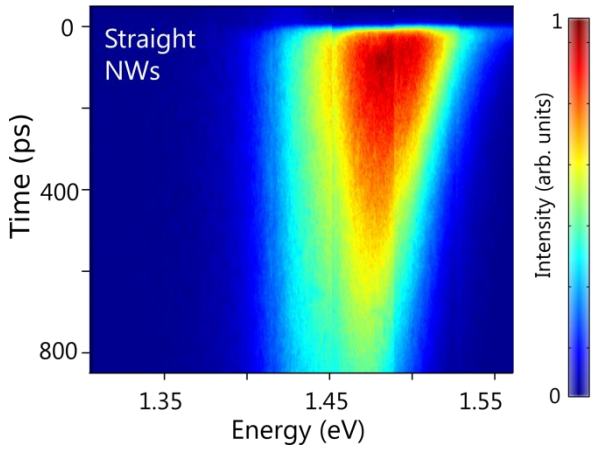


**Figure S7.** Streak camera image taken on straight GaAs/$Al_{0.3}Ga_{0.7}As$/$Al_{0.5}In_{0.5}As$ nanowires at 10 K.

## Optical anisotropy of bent nanowires

This section presents additional PL experiments carried out on straight and bent GaAs/$Al_{0.3}Ga_{0.7}As$/$Al_{0.5}In_{0.5}As$ core–multishell nanowires at room temperature, details the impact of bending on the polarization of the optical properties of the nanowires, and gives estimates of the enhancement of the light absorption cross section of bent nanowires compared to what is observed for planar samples.

### *1 - Antenna effect*

The polarization properties of light absorption and emission of semiconductor nanowires usually differ from that of the bulk. When the wavelength of light $\lambda$ is much larger than the nanowire diameter $d$, this modification in the polarization response is referred to as the antenna effect,[8] and arises from the continuity relations for the electric field $\boldsymbol{E}$ at the interfaces between the nanowire and its environment (usually air or vacuum). Figure S8 displays the intensity of the electric field $I_{in}$ in an infinitely long dielectric nanowire with a dielectric constant $\varepsilon = \varepsilon_r\varepsilon_0$, with $\varepsilon_r$ the relative dielectric constant and $\varepsilon_0$ the vacuum permittivity. Since $d \ll \lambda$, light can be treated as an electrostatic field. When light is polarized parallel to the nanowire axis, the electric field at the nanowire sidewalls is continuous and

$$I_{in} = I_{out} \qquad \text{Eq. (9),}$$

with $I_{out} = |\boldsymbol{E_0}|^2$ being the intensity of light far away from the nanowire. In contrast, for light polarized perpendicular to the nanowire, the electric field at the interfaces is discontinuous, $\boldsymbol{E}$ inside the nanowire is attenuated, and the ratio between $I_{in}$ and $I_{out}$ is given by:

$$\frac{I_{in}}{I_{out}} = \frac{4}{(\varepsilon_r+1)^2} \qquad \text{Eq. (10).}$$

As a result, straight as-grown nanowires measured in a backscattering geometry (the geometry used for all PL experiments in this work) do not exhibit any polarization response in light absorption and emission. In contrast, straight nanowires dispersed on a substrate and measured in backscattering geometry exhibit stronger light absorption and emission for light polarized parallel to the nanowire axis. The polarization anisotropy of a bent nanowire depends on the exact bending angle. It is therefore possible to control the polarization response of a bent-nanowire device by tuning the degree of bending.

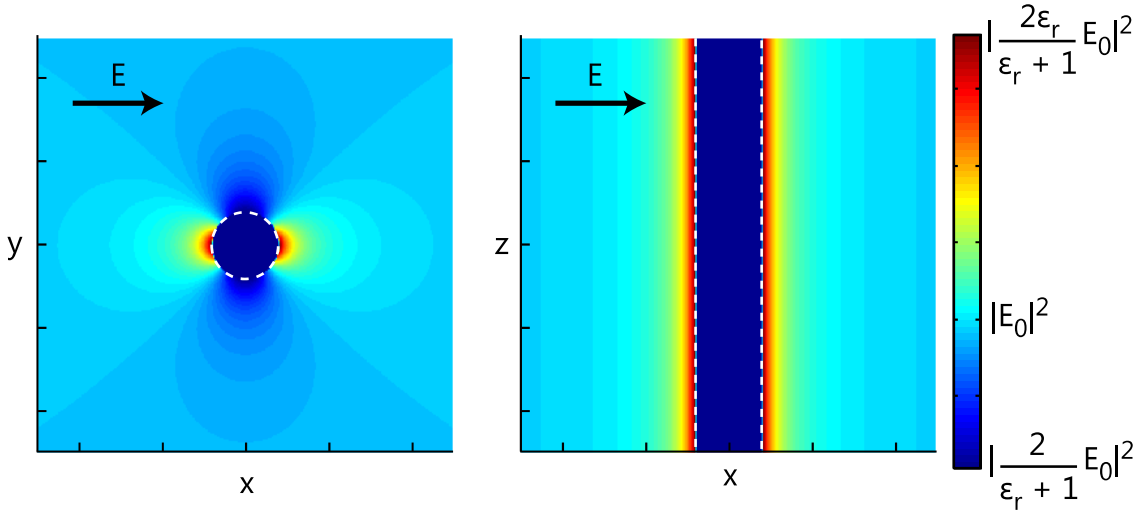


**Figure S8.** Field intensity distribution in an infinite nanowire in vacuum for light with a wavelength much larger than the nanowire diameter and polarized perpendicular to the nanowire axis. The intensity $I = |\boldsymbol{E}|^2$ is color-coded according to the scale bar on the right. The nanowire sidewalls are shown by white dashed lines in both panels. The wire and the light polarization are aligned along the *z* and *x* axes, respectively. For a GaAs nanowire (relative dielectric constant $\varepsilon_r$ = 13.1), the field intensity attenuation $I_{out}/I_{in}$ by the antenna effect is about 50.

### *2 - Impact of strain on the polarization of the photoluminescence of bent nanowires*

As shown in Figure 2f in the main text, the PL signal from the GaAs core of straight nanowires at 10 K is unpolarized, while that of bent nanowires is polarized along the bending axis. As the polarization anisotropy of light emission is similar to that of light absorption, we suggest that the linear polarization of the PL signal at 10 K is due to the antenna effect (see above). However, the variation in strain across the GaAs core of bent nanowires may affect the PL polarization even further. Figure S9 shows the variation in heavy-hole (HH) and light-hole (LH) bandgaps across the section of the GaAs core of a bent nanowire with a geometry similar to that described in Figure 2a. When the strain is compressive, the fundamental hole state in the GaAs core is the light-hole. In zincblende GaAs nanowires optical transitions involving heavy-holes are polarized perpendicular to the nanowire axis, while those involving light-holes are allowed for any polarization.[9] At 10 K, charge carriers drift toward the tensile-strained regions of the GaAs core where the fundamental valence band state is the heavy-hole. Consequently, the polarization anisotropy in the PL signal at 10 K is mostly related to the antenna effect. In contrast, at 300 K, charge carriers may occupy higher energy states at compressively strained regions of the core, where the fundamental hole is the light-hole.

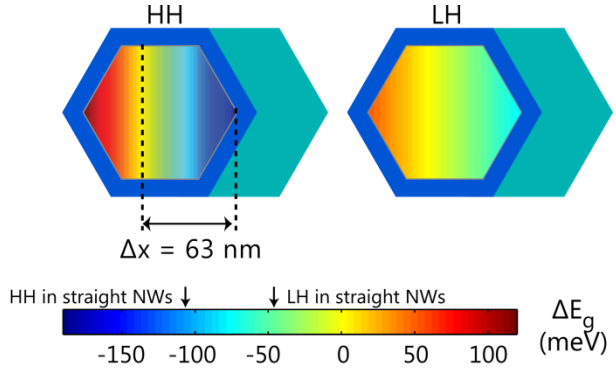


**Figure S9.** Heavy-hole (HH) and light-hole (LH) bandgap variation $\Delta E_g$ across the core of a bent GaAs/$Al_{0.3}Ga_{0.7}As$/$Al_{0.5}In_{0.5}As$ core–multishell nanowire. The blue and green regions correspond to the $Al_{0.3}Ga_{0.7}As$ and $Al_{0.5}In_{0.5}As$ shells, respectively. $\Delta E_g$ is color-coded according to the scale bar at the bottom. The HH and LH energies in a straight GaAs/$Al_{0.3}Ga_{0.7}As$/$Al_{0.5}In_{0.5}As$ core–multishell nanowire are also indicated. The HH is the fundamental hole state in the core region extending over $\Delta x$ = 63 nm and delimited with the two vertical dashed lines.

### *3 - Modeling the room-temperature photoluminescence of bent nanowires*

To quantify the impact of light-holes on the light emission properties of bent nanowires at 300 K, we have performed continuous-wave PL experiments. Figure S10a displays PL spectra taken on a reference GaAs epilayer and on the bent GaAs/$Al_{0.3}Ga_{0.7}As$/$Al_{0.5}In_{0.5}As$ core–multishell nanowires. Spectra taken on the straight nanowires with AlAs/GaAs/GaAs and $Al_{0.3}Ga_{0.7}As$/$Al_{0.5}In_{0.5}As$ outer shells are also shown. All spectra were acquired with an excitation power of 7 mW.

To extract the carrier density *n* for each sample, we perform PL lineshape fits. We first calculate the spontaneous emission rate *r*(*E*) using Fermi's golden rule. Assuming that the conduction and valence bands are parabolic, considering only vertical transitions in reciprocal space, and neglecting the split-off band, we obtain:

$$r(E) \propto \sum_{j=HH,LH} D_{cv}^{j}(E) f_e(E) f_j(E) \qquad \text{Eq. (11)}$$

where *HH* and *LH* stand for heavy-hole and light-hole, respectively, with the joint density of states $D_{cv}(E)$, and the Fermi–Dirac distributions for electrons and holes $f_e$ and $f_j$, respectively. For the planar and straight nanowire samples, $D_{cv}(E)$ was convoluted with a Gaussian with a linewidth equal to the PL linewidth at 10 K. For the bent-nanowire sample, $D_{cv}(E)$ was calculated using the strain distribution shown in Figure 2c and convoluted with a Gaussian with a linewidth equal to the PL linewidth of the straight GaAs/$Al_{0.3}Ga_{0.7}As$/$Al_{0.5}In_{0.5}As$ core–multishell nanowire sample at 10 K. The final state of the recombination has a finite lifetime due to Auger processes in the degenerate band. This finite lifetime leads to a broadening of the PL spectrum, which is accounted for by convoluting the PL spectrum with a Lorentzian of Landsberg type:[10]

$$\frac{1}{2\pi}\frac{\Gamma(E_1)}{(E-E_1)^2+[\Gamma(E_1)/2]^2} \qquad \text{Eq. (12)}$$

The half width at half maximum $\Gamma$ is given by:[11]

$$\Gamma(E_1) = \Gamma_0\left(1 - 2.229\frac{E_1}{E_F} + 1.458\left[\frac{E_1}{E_F}\right]^2 - 0.229\left[\frac{E_1}{E_F}\right]^3\right) \qquad \text{Eq. (13)}$$

with the Fermi level $E_F$, and the broadening factor at the bandgap $\Gamma_0$.[12] Finally, for the bent nanowires, we have also to account for the fact that the light wavevector is parallel and perpendicular to the nanowire axis when recombination occurs at the bottom and at the top of the nanowire, respectively.

The PL spectrum in Figure S10a taken on the GaAs epilayer is typical of bulk GaAs under high injection, and we deduce $n = 5\times10^{17}$ cm$^{-3}$ from the lineshape fit. The PL spectrum for the GaAs/AlAs/GaAs nanowires is blueshifted and exhibits a larger full width at half maximum (FWHM) compared to that of the epilayer, suggesting a higher $n$ in these nanowires. This finding is confirmed by a fit yielding $n = 1.1\times10^{19}$ cm$^{-3}$. Ensembles of straight nanowires thus exhibit a larger absorption cross section than planar layers, in agreement with results obtained in Refs.[13,14] The PL from the straight GaAs/$Al_{0.3}Ga_{0.7}As$/$Al_{0.5}In_{0.5}As$ core–multishell nanowires is not only redshifted compared to that of the GaAs/AlAs/GaAs nanowires, but also narrower. The FWHM for the PL spectra of these two samples are, however, similar at 10 K (Figure 2d). The fit in Figure S10a reveals that $n$ in straight GaAs/$Al_{0.3}Ga_{0.7}As$/$Al_{0.5}In_{0.5}As$ core–multishell nanowires is only $3.5\times10^{18}$ cm$^{-3}$. We note that the GaAs/AlAs/GaAs and straight GaAs/$Al_{0.3}Ga_{0.7}As$/$Al_{0.5}In_{0.5}As$ nanowires have different core–shell structures and different diameters (about 160 and 110 nm, respectively), which will result in different light couplings.

The best fit to the bent-nanowire PL spectrum in Figure S10a yields $n = 2.5\times10^{18}$ cm$^{-3}$. Therefore, bent nanowires present an absorption cross section five times larger than that of planar GaAs. In contrast to the observation made at 10 K in Figure 2d in the main text, straight and bent nanowires exhibit comparable PL peak energies at 300 K (Figure S10a). As shown in Figure S10b, this behavior is a result of the significant contribution of LH states to the PL spectra of bent GaAs/$Al_{0.3}Ga_{0.7}As$/$Al_{0.5}In_{0.5}As$ core–multishell nanowires. Bending thus promotes light emission from LH states, which is promising for various optoelectronic applications including nanowire-based low-threshold lasers[15] or quantum communication applications.[16]

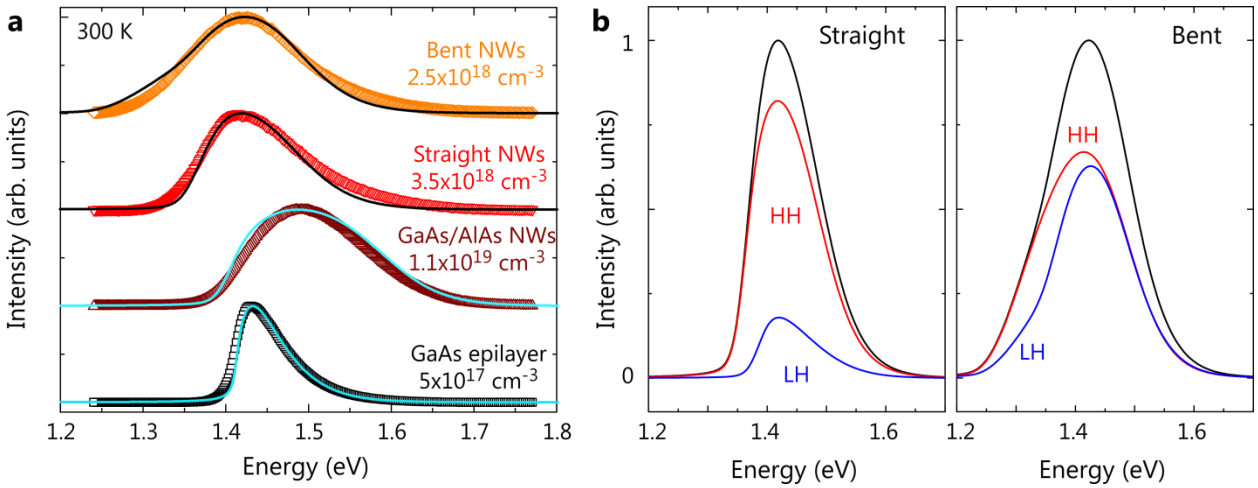


**Figure S10.** Modeling of room temperature PL spectra. (a) PL spectra taken on a GaAs epilayer, as well as on ensembles of GaAs/AlAs/GaAs core–multishell nanowires, and straight and bent GaAs/$Al_{0.3}Ga_{0.7}As$/$Al_{0.5}In_{0.5}As$ core–multishell nanowires, using the same excitation conditions. The spectra have been normalized and shifted vertically for clarity. The solid lines are the result of a fit of the PL lineshape. The injected carrier density *n* is a fitting parameter and is indicated on the right for each spectrum. The large *n* for the nanowire samples demonstrates that the absorption cross section is enhanced compared to the planar case. (b) The PL lineshape fit (black line) for the ensembles of straight and bent GaAs/$Al_{0.3}Ga_{0.7}As$/$Al_{0.5}In_{0.5}As$ core–multishell nanowires (left and right panels, respectively). The red and blue lines show the contribution of heavy-hole (HH) and light-hole (LH) transitions to the total spectra, respectively. The strong LH emission for the ensemble of bent nanowires is due to the combination of the antenna effect and charge carrier recombination in compressively strained regions of the GaAs core.

## References

(1) Loitsch, B.; Rudolph, D.; Morkötter, S.; Döblinger, M.; Grimaldi, G.; Hanschke, L.; Matich, S.; Parzinger, E.; Wurstbauer, U.; Abstreiter, G.; Finley, J. J.; Koblmüller, G. *Adv. Mater.* **2015**, *27* (13), 2195–2202.

(2) Lewis, R. B.; Corfdir, P.; Li, H.; Herranz, J.; Pfüller, C.; Brandt, O.; Geelhaar, L. *Phys. Rev. Lett.* **2017**, *119*, 086101.

(3) Lewis, R. B.; Corfdir, P.; Herranz, J.; Küpers, H.; Jahn, U.; Brandt, O.; Geelhaar, L. *Nano Lett.* **2017**, *17* (7), 4255–4260.

(4) Arciprete, F.; Placidi, E.; Magri, R.; Fanfoni, M.; Balzarotti, A.; Patella, F. *ACS Nano* **2013**, *7* (5), 3868–3875.

(5) Tixier, S.; Adamcyk, M.; Young, E. C.; Schmid, J. H.; Tiedje, T. *J. Cryst. Growth* **2003**, *251* (1–4), 449–454.

(6) Grandjean, N.; Massies, J.; Etgens, V. H. *Phys. Rev. Lett.* **1992**, *69* (5), 796–799.

(7) Harmand, J.-C.; Li, L. H.; Patriarche, G.; Travers, L. *Appl. Phys. Lett.* **2004**, *84* (20), 3981–3983.

(8) Wang, J.; Gudiksen, M. S.; Duan, X.; Cui, Y.; Lieber, C. M. *Science* **2001**, *293* (5534), 1455–1457.

(9) Spirkoska, D.; Efros, A. L.; Lambrecht, W. R. L.; Cheiwchanchamnangij, T.; Fontcuberta i Morral, A.; Abstreiter, G. *Phys. Rev. B* **2012**, *85* (4), 045309.

(10) Landsberg, P. T. *Phys. status solidi* **1966**, *15* (2), 623–626.

(11) Martin, R. W.; Störmer, H. L. *Solid State Commun.* **1977**, *22*, 523–526.

(12) Kappei, L.; Szczytko, J.; Morier-Genoud, F.; Deveaud, B. *Phys. Rev. Lett.* **2005**, *94* (14), 147403.

(13) Heiss, M.; Russo-Averchi, E.; Dalmau-Mallorquí, a; Tütüncüoğlu, G.; Matteini, F.; Rüffer, D.; Conesa-Boj, S.; Demichel, O.; Alarcon-Lladó, E.; Fontcuberta i Morral, A. *Nanotechnology* **2014**, *25* (1), 14015.

(14) Corfdir, P.; Küpers, H.; Lewis, R. B.; Flissikowski, T.; Grahn, H. T.; Geelhaar, L.; Brandt, O. *Phys. Rev. B* **2016**, *94* (15), 155413.

(15) Adams, A. R. *Electron. Lett.* **1986**, *22* (5), 249.

(16) Huo, Y. H.; Witek, B. J.; Kumar, S.; Cardenas, J. R.; Zhang, J. X.; Akopian, N.; Singh, R.; Zallo, E.; Grifone, R.; Kriegner, D.; Trotta, R.; Ding, F.; Stangl, J.; Zwiller, V.; Bester, G.; Rastelli, A.; Schmidt, O. G. *Nat. Phys.* **2013**, *10* (1), 46–51.